Ion acceleration by beating electrostatic waves: Domain of allowed acceleration

R. Spektor and E. Y. Choueiri
Electric Propulsion and Plasma Dynamics Laboratory (EPPDyL), Princeton University, Princeton, New Jersey 08544, USA
(Received 15 September 2003; published 14 April 2004)

The conditions under which a magnetized ion can be accelerated through a nonlinear interaction with a pair of beating electrostatic waves are explored. It has been shown [Benisti *et al.*, Phys. Plasma 5, 3224 (1998)] that the electric field of the beating waves can, under some conditions, accelerate ions from arbitrarily low initial velocity in stark contrast with the well-known nonlinear threshold criteria for ion acceleration by a single wave. It is shown here that the previously found condition is necessary but not sufficient for acceleration to occur. The sufficient *and* necessary conditions are identified in terms of the location of the critical points of the motion on the Poincaré section. A second-order perturbation analysis was carried out to approximate the location of these critical points and define the domains of allowed and forbidden acceleration. It is shown that for an ion to be significantly energized, the Hamiltonian must be outside the energy barrier defined by the location of the elliptic and hyperbolic critical points. Despite the restriction on the Hamiltonian, an ion with arbitrarily low initial velocity may benefit from this acceleration mechanism.

DOI: 10.1103/PhysRevE.69.046402 PACS number(s): 52.65.Cc, 52.20.Dq, 05.45.Pq, 94.20.Rr

I. INTRODUCTION

Ion heating by a spectrum of electrostatic waves propagating perpendicularly to the magnetic field was proposed by Ram *et al.* [1] in 1998 as an explanation for ionospheric ion heating observed by the Topaz 3 rocket. In the same year Benisti *et al.* demonstrated that ions with an arbitrary low initial velocity can be accelerated through a nonlinear interaction with the waves whenever the spectrum contains a pair of waves that obey a beating criterion: their frequencies must differ by an integer number of the ion cyclotron frequency [2,3]:

$$\omega_2 - \omega_1 = n\omega_c . \tag{1}$$

Because of the lack of a threshold for the initial ion velocity, this acceleration mechanism promises to energize a larger portion of the ion distribution function. Therefore, it may be promising to many applications where the efficiency of ion heating is of prime importance, such as plasma heating in fusion devices and spacecraft plasma propulsion.

A preliminary numerical exploration [4] of this mechanism revealed that there are many cases for which the beating criterion (1) does *not* lead to ion acceleration. This hinted to the possibility that the criterion is necessary but not sufficient.

In this paper we define the necessary *and* sufficient conditions for the acceleration of a magnetized ion through nonlinear interaction with a pair of propagating electrostatic waves. In particular, we analyze the Poincaré section of the ion's motion [5] and show that the dynamics of the ion acceleration is determined by the critical points of the motion [6]. These critical points were not observed in previous studies [2,3] since these studies were limited to the analysis of a single trajectory (i.e., a single initial condition) in a given Poincaré section. The location of the critical points, which can only be seen when multiple ion trajectories are analyzed, allows us to define the necessary and sufficient condition for acceleration.

In Sec. II we review previous relevant work. In Sec. III we overview the analytical formulation of the problem. In Sec. IV we describe the construction and interpretation of the graphic solutions. We solve the equation of the ion's motion numerically in Sec. V to show how critical points influence its dynamics. In the remaining sections we seek analytical expressions for the location of the critical points of the motion, which amount to a definition of the domains of allowed and forbidden acceleration.

II. REVIEW OF PREVIOUS WORK

Stochastic heating of a magnetized ion by a single propagating electrostatic (ES) wave has been extensively studied [8–11]. Using first-order perturbation theory Karney [7,10] was able to derive analytical expressions approximating overall nonlinear dynamics of an ion interacting with a single ES wave. That work revealed the existence of a threshold for the initial ion energy below which the particle cannot gain net energy from the ES wave. This threshold can be expressed in terms of the ion's velocity as

$$v_{th} = \frac{\omega}{k} - \sqrt{\frac{qE}{km}}, \tag{2}$$

where v_{th}, m, and q are the velocity, mass, and charge of the ion, and ω, k, and E are the frequency, wave number, and electric field amplitude of the wave. Skiff *et al.* validated these findings experimentally [12]. The significance of the threshold can be seen from the example demonstrated in Fig. 1. It shows the typical velocity evolution of two test ions obtained through numerical simulation. Below the threshold, indicated by the horizontal dashed line, we observe that the ion motion is regular, and consequently we can predict its behavior well by means of perturbation theory. More importantly, as long as the ion's initial velocity is in that region the

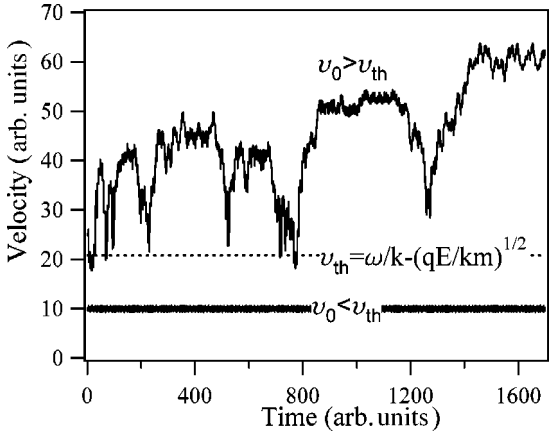

FIG. 1. Time evolution of the velocity for a particle interacting with a single wave. The threshold derived in Ref. [7] and given by Eq. (2) represents the boundary between the regular and stochastic domains, and is shown as a horizontal dashed line.

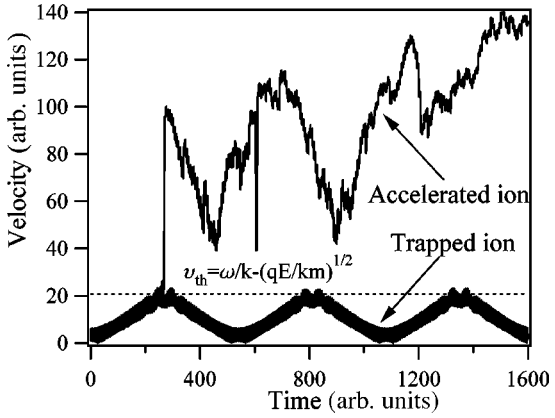

FIG. 2. Time evolution of the velocity for a particle interacting with two beating waves. Two particle trajectories are shown, one with an ion trapped below the $v_{th} < \omega/k - \sqrt{qE/km}$ threshold, and another resulting in an accelerating ion. For both trajectories the initial velocities are the same (but the initial cyclotron angle is different).

ion will not gain a net energy from the wave [7]. When the initial velocity is above the threshold, the ion moves stochastically and eventually gains a net energy, as shown by the upper trajectory in Fig. 1. As shown by Karney [7], in the case of interaction with a *single* wave the ion gains energy only chaotically when its initial velocity exceeds the threshold. Thus the threshold separates two regions of phase space: a *regular* (or coherent) motion region of low energies below the threshold and a *stochastic* one — above the threshold. Nonlinear ion acceleration by a single wave is therefore always a stochastic process.

In 1998 Benisti and co-workers described a fundamentally different mechanism for nonlinear ion acceleration by ES waves [1–3]. The scheme requires *pairs* of ES waves that obey a beating criterion described by Eq. (1). Under such conditions the single-wave theory threshold disappears and *regular* and *stochastic* regions of phase space become connected, allowing ions with arbitrarily small initial velocities to obtain high energies through coherent acceleration followed by stochastic energization.

Subsequently, we performed numerical investigation [4] based on the same single trajectory method and found that some initial conditions did *not* lead to ion acceleration even if condition (1) was satisfied, as illustrated in Fig. 2. This implied that condition (1) may be necessary but not sufficient. We concluded that to find the necessary *and* sufficient conditions for ion acceleration we need to examine the complete Poincaré section using multiple trajectories and find the critical points of motion, as will be done in Secs. V and VI.

III. ANALYTICAL FORMULATION

We start by defining the coordinate axis as shown in Fig. 3. Here we have a single ion of mass m and charge q in a constant and homogeneous magnetic field, $\mathrm{B}_0\hat{z}$. This ion interacts with a packet of electrostatic waves that propagate in the positive x direction. Since we take the waves to be purely electrostatic the wave number k_i is parallel to the electric field E_i of each of these waves. The dynamics of the single ion in Fig. 3 is described by the following equation of motion [2,13]:

$$\frac{d^2x}{dt^2} + \omega_c^2 x = \frac{q}{m} \sum_i E_i \sin(\mathrm{k}_i x - \omega_i t + \varphi_i), \tag{3}$$

where $\omega_c = q\mathrm{B}_0/m$ is the ion cyclotron frequency and φ_i is the phase angle of each wave. The corresponding Hamiltonian for the system is [2]

$$\overline{H} = \rho^2/2 + \sum_i \frac{\varepsilon_i}{\kappa_i} \cos(\kappa_i \rho \sin\theta - \nu_i \tau + \varphi_i). \tag{4}$$

In writing Eq. (4) we have used the fact that the system is periodic, and transformed the Hamiltonian into normalized action-angle coordinate system [14], where $\kappa_i = k_i/k_1$, $\nu_i = \omega_i/\omega_c$, $\tau = \omega_c t$, $\varepsilon_i = (\mathrm{k}_1 q E_i)/(m\omega_c^2)$, $\rho^2 = X^2 + \dot{X}^2$, and $X = k_1 x$, $\dot{X} = dX/d\tau$, so that $X = \rho \sin\theta$, $\dot{X} = \rho\cos\theta$. The action-angle coordinate system is a special case of polar coordinates [5]. In our context θ corresponds to the cyclotron phase angle measured clockwise from the y axis, as indicated

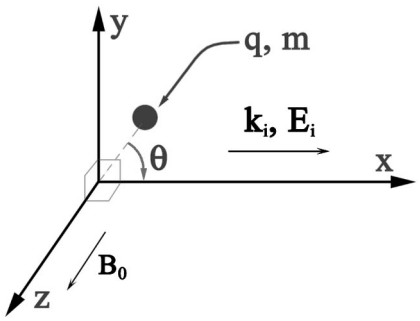

FIG. 3. A single ion of charge q and mass m in a constant homogeneous magnetic field $\mathrm{B}_0\hat{z}$ interacts with a spectrum of electrostatic waves whose wave-number and electric field direction is parallel to the x axis.

in Fig. 3, while ρ is the normalized Larmor radius which, in a constant magnetic field, represents the normalized velocity (perpendicular to the magnetic field) of the magnetized particle undergoing cyclotron motion in the *xy* plane. When ν_i are exactly an integer multiple of the ion cyclotron frequency we speak of an *on-resonance* wave; otherwise it is *off-resonance*.

Benisti *et al.* [2] defined a criterion for particle acceleration by multiple ES waves. They showed that for regular and stochastic regions to be connected it is necessary (but, as we shall see, not sufficient) to have at least one pair of ES waves such that

$$\nu_2 - \nu_1 = n, \tag{5}$$

where n is an integer. They also report that acceleration is more vigorous for $n \leqslant 2$, therefore for the sake of simplicity, we limit our analysis to the case of a single pair of beating waves, such that $n=1$. In addition, Ref. [2] reports that the maximum acceleration is achieved when all waves are of the same amplitude, $\varepsilon_i = \varepsilon_j = \varepsilon$. We also set $\kappa_i = \kappa_j = \kappa_1$ to simplify our analysis, and since the phase angles φ_i do not play a fundamental role in this acceleration process [2] we set all $\varphi_i = 0$. With these simplifications the Hamiltonian (4) becomes

$$\overline{H} = \rho^2/2 + \varepsilon[\cos(\rho \sin\theta - \nu_i \tau) + \cos(\rho \sin\theta - \nu_j \tau)]. \tag{6}$$

This Hamiltonian represents two coupled oscillators: one is the gyrating ion and the other corresponds to the beating ES waves. We, therefore, can interpret ε as a coupling parameter between the two oscillators.

The detailed derivation of the analytical solution for a particle interacting with a single wave can be found in Ref. [7]. However, a more generalized solution for multiple waves is obtained [13,15,16] through Deprit's modified Lie transformation in Refs. [2,3]. The resulting autonomous Hamiltonian derived from Eq. (6) for a *noninteger* value of ν to the second order in the perturbation, ε, is

$$\begin{aligned} H = {} & \varepsilon\{J_{\nu_i}(\rho)\cos(\nu_i\theta) + J_{\nu_j}(\rho)\cos(\nu_j\theta)\} \\ & + \varepsilon^2\{S_1^{\nu_i}(\rho) + S_1^{\nu_j}(\rho) + S_6^{\nu_i,\nu_j}(\rho)\cos[(\nu_j - \nu_i)\theta]\}, \end{aligned} \tag{7}$$

where

$$\begin{aligned} S_1^{\nu_i}(\rho) &= \frac{1}{2\rho}\sum_{m=-\infty}^{\infty}\frac{m J_m(\rho) J_m'(\rho)}{\nu_i - m}, \\ S_6^{\nu_i,\nu_j}(\rho) &= \frac{1}{2\rho}\left(\sum_{m=-\infty}^{\infty}\frac{m J_m(\rho) J'_{\nu_j-\nu_i+m}(\rho)}{\nu_i - m} + \sum_{m=-\infty}^{\infty}\frac{m J_m(\rho) J'_{\nu_i-\nu_j+m}(\rho)}{\nu_j - m}\right). \end{aligned} \tag{8}$$

J_m is the Bessel function of the first kind of order m, and J' represents the derivative of the Bessel function with respect to its argument. When ν_i is an integer, the summations are performed over all $m \neq \nu_i$ to avoid singularities. When $\nu \neq$ integer, the first-order terms in Eq. (7) disappear [2], and the equation becomes more tractable.

We now explore particle dynamics as a function of wave amplitude and frequency, and in terms of the location of critical points on the phase diagrams. Solving Eq. (6) numerically we will demonstrate that when critical points are absent in the regular region of the phase diagram (as in the single wave-particle interaction), the particle will not gain net energy.

IV. GRAPHICAL ANALYSIS

A convenient way of representing both numerical and analytical solutions is to plot the resulting trajectories on a Poincaré section [5]. To construct a Poincaré section from the numerical integration of Eq. (6) we plot the point intersections of the ion trajectory in three dimensions (ρ, θ, τ) with the ρ-θ plane at specific time intervals. For integer values of ν this reduces to plotting ρ vs θ at $\tau = 2\pi j$, where $j = 0,1,2, \ldots$ is a nonnegative integer. For noninteger values of ν precaution must be taken for a proper accounting of intersection points. Since the magnetic field is constant, the normalized cyclotron radius ρ is a direct measure of the perpendicular ion velocity. Therefore Poincaré sections give direct visual insight into the acceleration process.

In constructing the Poincaré section from the analytical solution we note that the Hamiltonian in Eq. (7) is autonomous, and therefore itself is an invariant of motion. Curves of constant H in a Poincaré section represent the complete analytical solution of the problem to second order.

The visual interpretation of Poincaré sections is straightforward. A random point distribution corresponds to stochastic motion while regular patterns, such as lines and ellipses, will tell us that the ion dynamics is analytical (or regular). For example, if the wave amplitude ε is zero, Eqs. (3) and (6) reduce to a simple harmonic oscillator and for irrational values of ν its Poincaré section shows a set of horizontal lines, indicating a constant velocity (which corresponds to a free ion gyrating in a constant magnetic field). Each of these lines represents an invariant of motion for a given set of initial conditions [5]. When the coupling parameter ε is not zero, we can treat the ion motion as a perturbation of these invariants.

As with most phase diagrams, critical points define the dynamics of the motion. Since the system is not dissipative we expect to find two types of critical points: elliptic and hyperbolic. As we shall show later, the location of the critical points is the key to determining which initial conditions lead to acceleration or trapping. The task before us is to find these critical points. Our research is guided by a comparison of the Poincaré sections of the analytical solution to those obtained through numerical integration of Eq. (6). It should be noted that we should not expect to see any stochastic behavior on the Poincaré sections obtained from the analytical solution.

V. TOPOLOGY OF THE POINCARÉ SECTION

In Fig. 4 we show typical Poincaré sections obtained by numerical integration for $\nu_1 = 24.3$ and $\nu_2 = 25.3$. The panels

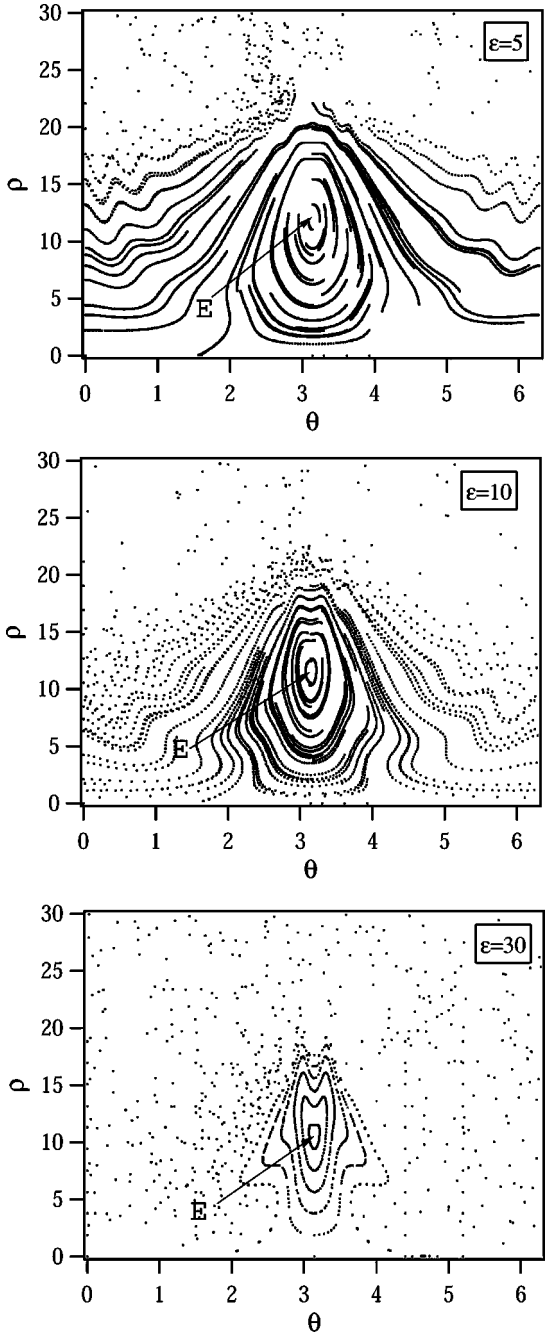

FIG. 4. Poincaré sections showing numerical solutions for a particle interacting with two beating off-resonance waves ($\nu_i=24.3$ and $\nu_j=25.3$). The stochastic region occupies a greater fraction of the phase space as the wave amplitude is increased.

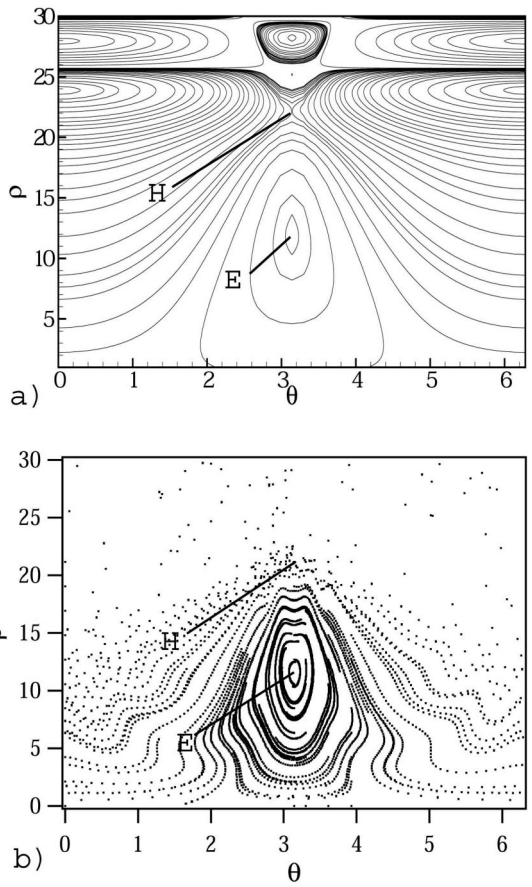

FIG. 5. Poincaré section for a particle interacting with two beating off-resonance waves ($\varepsilon=10$, $\nu_i=24.3$, and $\nu_j=25.3$). (a) Analytical solution showing the existence of hyperbolic and elliptic points marked by *H* and *E*, respectively. (b) Numerical solution also showing the locations of the critical points.

in this figure illustrate the effect of increasing wave amplitude. The phase diagram consists of two regions, stochastic and regular, just as for the single wave interaction. However, unlike the single wave-ion interaction, the two regions are ''connected.'' By ''connected'' we mean that an ion with low initial velocity can undergo first regular and then stochastic acceleration, reaching high energies.

For low perturbation strength (low values of ε) the regular region extends to values of ρ approximately predicted by Eq. (2). However, as ε is increased the regular region quickly shrinks to the vicinity of the elliptic critical point (designated *E* in Fig. 4). Notice that the elliptic point is located at $\rho_E \sim \nu/2$ and $\theta_E=\pi$. Eventually, as the wave amplitude is raised above values shown in Fig. 4, chaotic motion dominates the phase diagram.

We now gauge how well the second-order perturbation analysis compares to the numerical solutions. Figure 5 indicates a good degree of agreement between the two. Even though the detailed structure of the regular motion lines is not captured with the analytical solution, the latter does predict the position of the lower elliptic (*E*) as well as the hyperbolic point (*H*) rather well. On the other hand, our analytical approach breaks down in the stochastic region, as should be expected. Therefore the critical points shown by the analytical solution to be at $\rho>25$ in Fig. 5(a) (which can be said to describe a ''homoclinic tangle'' or ''stochastic layer'') are in reality covered by the stochastic motion, as shown by the numerical solution. However, as described in Ref. [3], even in that region of phase space the overall ion motion could be approximated by first-order orbits, for small ε.

In the case of a particle interacting with beating waves we are mainly concerned with the hyperbolic and elliptic critical points designated *H* and *E*, respectively, in Fig. 5. It is clear

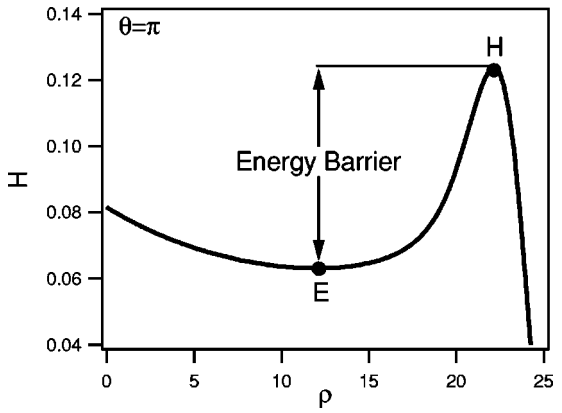

FIG. 6. Analytical Hamiltonian as a function of ρ at $\theta=\pi$. The elliptic and the hyperbolic points corresponding to the ones shown in Fig. 5 are the minimum and maximum of H ($\nu_i=24.3$ and $\nu_j=25.3$).

by tracing trajectories in Figs. 4 and 5 that an ion whose Hamiltonian lies between the Hamiltonian values corresponding to points E and H does not gain net energy from the waves i.e., does not reach the stochastic region where it can be vigorously accelerated. Instead the corresponding phase space trajectories circulate around the elliptic critical point E or cover the full range of cyclotron phase angles ($0\leqslant\theta\leqslant 2\pi$) while remaining below H.

It is relevant to note in this context that the Hamiltonian of various trajectories increases monotonically from the Hamiltonian value at point E to its value at point H, as shown in Fig. 6. The figure shows the Hamiltonian determined from Eqs. (7) and (8) as a function of ρ for $\theta=\pi$ and illustrates that the location of the *elliptic* and the *hyperbolic* points could be found by determining the local minimum and the maximum of H.

Therefore, for given values of ν_i and ε, the inequality

$$H_E<H(\rho_0,\theta_0)<H_H \quad \text{with} \quad \rho_0<\nu-\sqrt{\varepsilon} \tag{9}$$

defines the *forbidden acceleration domain*, where H_E and H_H are the Hamiltonian values for the elliptic (E) and the hyperbolic (H) points, and the subscript "0" refers to initial conditions. By "forbidden acceleration domain" we mean here the domain of initial conditions for which an ion cannot reach the stochastic region of phase space where it can be vigorously energized. This shows that not all ions will be accelerated by the waves even when the beating criterion (1) is satisfied. All other ion trajectories then lie in the *allowed acceleration domain* of phase space. The ions in the allowed acceleration domain will be affected by the waves strongly. The restriction on ρ_0 in Eq. (9) is needed because ions with $\rho_0\gtrsim\nu-\sqrt{\varepsilon}$ will not be trapped in the energy barrier between the elliptic and the hyperbolic points (i.e., in the forbidden acceleration domain), as shown in Fig. 6.

The "trapping" criterion in Eq. (9) given in terms of the Hamiltonian should be contrasted with the threshold criterion for interaction with a single wave given by Eq. (2). It is clear that, unlike the single-wave case, an ion with initial velocity ρ_o below the "threshold" can still be accelerated to high energies if the corresponding Hamiltonian is outside the range described by Eq. (9).

From the point of view of plasma acceleration one would like to limit the number of particles trapped in the forbidden acceleration domain ($H_E<H(\rho_0,\theta_0)<H_H$). The rest of the ions gain much higher energies through first regular (if their initial energy is low) and then stochastic acceleration, as shown in Figs. 4 and 5. However, even the trapped particles can escape into the stochastic domain as could happen through elastic scattering in a collisional plasma. We have studied this effect through particle simulations reported in Ref. [17].

VI. CRITICAL POINTS

To define the domains of allowed and forbidden acceleration described by Eq. (9) we need to find the location of the critical points E and H. We now seek analytical expressions for both.

Since both points are the extrema of the Hamiltonian, that task can be achieved by setting the time derivative of ρ and θ to zero simultaneously [5,6]. Utilizing Hamilton's equations of motion in conjunction with Eqs. (7) and (8) we get

$$\dot{\rho}=\frac{\partial H}{\partial\theta}=\varepsilon\{\nu_i J_{\nu_i}(\rho)\sin(\nu_i\theta)+\nu_j J_{\nu_j}(\rho)\sin(\nu_j\theta)\}$$
$$+\varepsilon^2(\nu_i-\nu_j)S_6^{\nu_i,\nu_j}(\rho)\sin[(\nu_j-\nu_i)\theta]=0, \tag{10}$$

$$\dot{\theta}=-\frac{\partial H}{\partial\rho}=\varepsilon\{J'_{\nu_i}(\rho)\cos(\nu_j\theta)+J'_{\nu_j}(\rho)\cos(\nu_j\theta)\}$$
$$+\varepsilon^2\{S_1'^{\nu_i}(\rho)+S_1'^{\nu_j}(\rho)+S_6'^{\nu_i,\nu_j}(\rho)$$
$$\times\cos[(\nu_i-\nu_j)\theta]\}=0. \tag{11}$$

When both wave frequencies are off-resonance ($\nu_i,\nu_j\neq$ integer), the equations above simplify because the first-order terms drop out, and we are able to obtain the position of critical points analytically.

For $\nu\neq$ integer, the $S_1^{\nu_i}(\rho)$ term in Eq. (8) could be simplified to an algebraic equation containing only a few Bessel functions [13]:

$$S_1^{\nu_i}(\rho)=\frac{\pi}{8\sin\nu_i\pi}[J_{\nu_i+1}(\rho)J_{-(\nu_i+1)}(\rho)$$
$$-J_{\nu_i-1}(\rho)J_{-(\nu_i-1)}(\rho)]. \tag{12}$$

As a result of this simplification we can reduce the $S_6^{\nu_i,\nu_j}(\rho)$ term down to

$$S_6^{\nu_i,\nu_j}(\rho)=\frac{\rho}{\nu_i}S_1^{\nu_i}(\rho)+\frac{\rho}{\nu_j}S_1^{\nu_j}(\rho). \tag{13}$$

The details of this derivation are given in the Appendix. We can therefore express Hamiltonian (7) in terms of the simplified $S_1^{\nu_i}(\rho)$ function only:

$$H=\varepsilon^2\left\{\left(1+\frac{\rho}{\nu_i}\cos[\nu_i-\nu_j]\theta\right)S_1^{\nu_i}(\rho)+\left(1+\frac{\rho}{\nu_j}\cos[\nu_i-\nu_j]\theta\right)S_1^{\nu_j}(\rho)\right\}. \quad (14)$$

As we will show later in this section our analysis breaks down for small values of ν. Consequently we take $\nu_i \gg 1$, and remembering that $n=1$ with $\rho/\nu_j=\rho/(\nu_i+1)\sim\rho/\nu_i(1-1/\nu_i^2+\cdots)$ we can approximate $\rho/\nu_i\sim\rho/\nu_j$. Dropping the subscripts in $S_1^{\nu_i}(\rho)$ we have

$$H=\varepsilon^2\left[1+\frac{\rho}{\nu_i}\cos(\nu_i-\nu_j)\theta\right]\times[S^{\nu_i}(\rho)+S^{\nu_j}(\rho)]. \quad (15)$$

Finally, we substitute Eq. (12) for each of the $S_1^{\nu_i}(\rho)$ functions. Expressing everything in terms of ν_i we get

$$H=\frac{\varepsilon^2\pi}{8\sin\nu\pi}\left(1+\frac{\rho}{\nu}\cos\theta\right)[-J_{\nu-1}(\rho)J_{-(\nu-1)}(\rho)+J_\nu(\rho)J_{-\nu}(\rho)+J_{\nu+1}(\rho)J_{-(\nu+1)}(\rho)-J_{\nu+2}(\rho)J_{-(\nu+2)}(\rho)], \quad (16)$$

where we have replaced ν_i with ν.

We are now ready to find the position of points E and H. From Eq. (10) as well as from Figs. 4 and 5 we see that these points lie at $\theta=\pi$. This reduces Eqs. (10) and (11) to

$$\frac{\partial}{\partial\rho}\left(1-\frac{\rho}{\nu}\right)L(\rho)=0,$$

where

$$L(\rho,\nu)=-J_{\nu-1}(\rho)J_{-(\nu-1)}(\rho)+J_\nu(\rho)J_{-\nu}(\rho)+J_{\nu+1}(\rho)J_{-(\nu+1)}(\rho)-J_{\nu+2}(\rho)J_{-(\nu+2)}(\rho). \quad (17)$$

From Eq. (17) we can express ρ as a function of $L(\rho)$ and $L'(\rho)$, where the prime denotes the derivative with respect to ρ, and arrange the resulting expression as

$$\frac{\rho}{\nu}=1-\frac{1}{\nu}\frac{L(\rho,\nu)}{L'(\rho,\nu)} \quad (18)$$

or

$$F(\rho,\nu)\equiv 1-\frac{\rho}{\nu}-\frac{1}{\nu}\frac{L(\rho,\nu)}{L'(\rho,\nu)}=0. \quad (19)$$

The first and second roots of Eq. (19), ρ_E and ρ_H, for a given value of ν, correspond to the locations of the *elliptic* and *hyperbolic* points respectively.

The solution to Eq. (18) for a range of ν is shown in Fig. 7, while the $F(\rho,\nu)$ of Eq. (19) is plotted as a function of ρ/ν for $\nu\in[55.001,55.999]$ in Fig. 8. It is now important to discuss the behavior of these solutions.

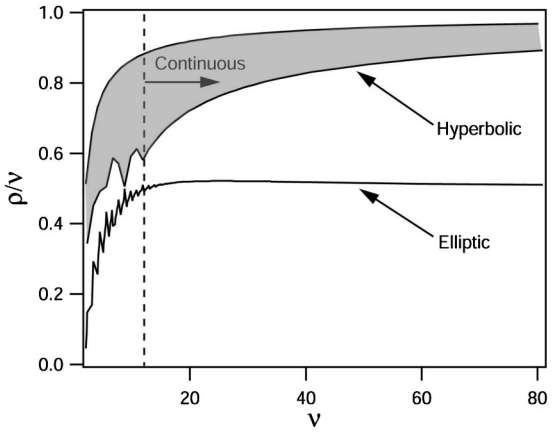

FIG. 7. Solution to Eq. (18) as a function of ν. The elliptic and hyperbolic points, E and H, could not always be found for small ν. For $\nu>9$ both points could be found for any values of ν. That region is marked as ''continuous'' on the figure.

As we discussed above, we are only considering the cases with $\nu\neq$ integer. Unfortunately, due to the asymptotic behavior of the Bessel function near the ''turning point'' [18], defined as $\rho_{tp}=\sqrt{\nu(\nu+1)}$, the solution approaches different limits as ν gets close to an integer from different sides. This peculiar behavior is demonstrated for the case of $\nu\sim 55$ in Fig. 8. Therefore, no simple analytical expression could be obtained for the position of the hyperbolic point. Instead, Fig. 7 shows a range of solutions for the location of this point. On the other hand, the elliptic point is very well defined. It is seen that for sufficiently large values of ν the location of the elliptic point, according to our second-order perturbation analysis is at

$$\rho_E\simeq\frac{\nu}{2},\quad \theta_E=\pi. \quad (20)$$

Although no simple expression could be found for the location of the hyperbolic point, we see from Fig. 7 that its

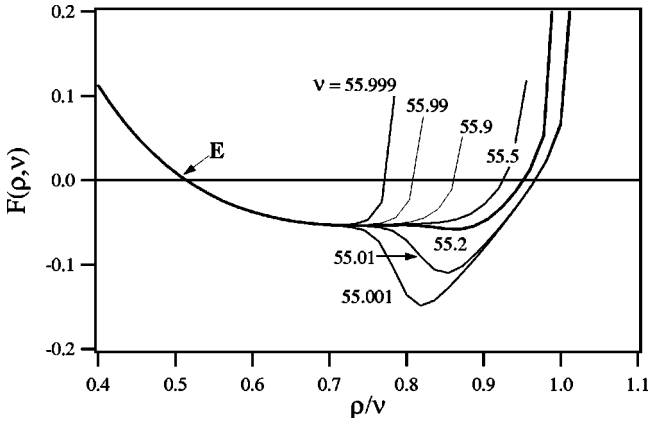

FIG. 8. Plot of the function $F(\rho,\nu)$, given by Eq. (19), showing how the second root (corresponding to the hyperbolic point) moves away from $\rho/\nu=1$ as ν changes from 55.001 to 55.999. The first root on the left, marked E, represents the elliptic point and the subsequent roots represent the hyperbolic points for the various values of ρ/ν.

location asymptotes (at large values of ν) to a value of $\rho/\nu \sim 0.8$–1.0; therefore we may approximate

$$\rho_H \simeq 0.9\nu, \quad \theta_H = \pi. \tag{21}$$

It is also important to mention that because of the asymptotic behavior of Bessel functions, the elliptic and hyperbolic points could not always be found for small values of ν. For these cases while the expression for the Hamiltonian [Eq. (16)], is still valid, our analysis of the allowed and forbidden acceleration domains does not apply. The range of ν for which we could always find both critical points is designated as ''continuous'' in Fig. 7.

Another limitation is placed on our analysis by its independence on ε in locating the critical points, as seen from Eq. (17). Extensive ($\varepsilon \approx 5-100$, $\nu \approx 10-50$) numerical exploration of the weak dependence of the critical point locations on ε suggests the following corrections to expressions (20) and (21), which are reminiscent of the ε dependence in the single wave interaction [7] [Eq. (2)],

$$\rho_E \simeq \frac{(\nu - \sqrt{\varepsilon})}{2}, \quad \theta_E = \pi, \tag{22a}$$

$$\rho_H \simeq \nu - \sqrt{\varepsilon}, \quad \theta_H = \pi. \tag{22b}$$

The physical interpretation and significance of these two points could be understood as follows. Looking back at Fig. 3 we see that both points correspond to the particles moving 180° out of phase with the electric field of the wave. We can note from Fig. 6 that at the hyperbolic point the ion velocity is $v_H = -\omega/k + v_{tr}$ (v_{tr} is the trapping velocity defined by the second term of Eq. (2) [7]) and the Hamiltonian is at the maximum, while at the elliptic point the ion velocity is $v_E = (-\omega/k + v_{tr})/2$, and the Hamiltonian is at the minimum. The difference in the Hamiltonian of the two points then forms an ''energy barrier,'' which an ion must overcome to be accelerated by the wave.

Another way to understand the importance of the elliptic point is to realize that at this point the energy exchange between the ion and the waves is minimum and the situation is equivalent to stable equilibrium for a pendulum. Any small perturbation from that equilibrium will only cause small oscillations about it. This implies that in the immediate neighborhood of point E the ion energy cannot be altered sufficiently to push the ion into the stochastic region, as seen in Fig. 5. On the other hand, the hyperbolic point corresponds to the unstable equilibrium of the pendulum and any small perturbation from it will cause significant changes in the ion motion, i.e. escape into the stochastic region and subsequent vigorous heating.

VII. BEATING WAVES (ON-RESONANCE)

When we choose ν_i and ν_j to be both on-resonance, the overall behavior becomes much more complicated and no simple analytical expression, as in the previous section, can be found. Figure 9 shows a typical example, the case with $\varepsilon = 10$, $\nu_i = 24$, and $\nu_j = 25$. One of the major differences

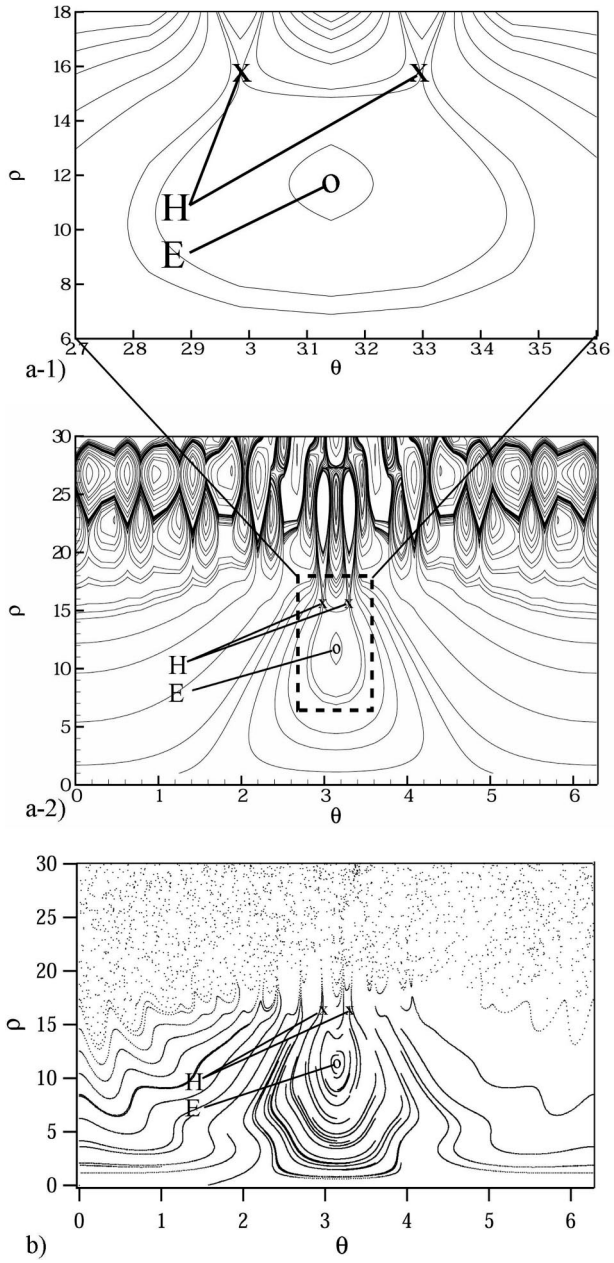

FIG. 9. Poincaré section for a particle interacting with two beating on-resonance waves showing a more complicated picture than that of the off-resonance case shown in Fig. 5. ($\varepsilon = 10$, $\nu_i = 24$, $\nu_j = 25$). (a-1) and (a-2) analytical solutions. (b) Numerical solution.

with respect to the off-resonance case is that now we have two hyperbolic points which do not lie at $\theta = \pi$. Nevertheless, we could still find their positions by solving Eqs. (10) and (11) numerically.

The location of the elliptic point is easier to obtain since the first-order terms in Eqs. (10) and (11) drop out for $\theta = \pi$, as in the off-resonance case. Also, Fig. 9 shows that the analytical solution exhibits much more complicated chains of the critical points at large values of ρ. While in reality these points are ''inside'' the stochastic region, this graphical picture illustrates why the analytical treatment of the on-resonance case is more challenging. However, we note that

the locations of both the elliptic and the hyperbolic points even in this case are very close to those determined by Eqs. (22). Indeed, by studying numerically the solutions to Eq. (6) for both on-resonance and off-resonance cases we conclude that the locations of elliptic and hyperbolic points for both cases could be well predicted by Eqs. (22).

VIII. SUMMARY AND CONCLUDING REMARKS

The beating criterion ($\omega_1-\omega_2=n\omega_c$) proposed by Benisti *et al*. [2,3] can allow a magnetized ion to be energized by a pair of beating electrostatic waves. The importance of this mechanism stems from its ability to accelerate ions with arbitrarily low initial velocity. It has become clear, however (see Fig. 2), that this criterion is not sufficient for acceleration.

In order to better define the criteria for acceleration we investigated multiple ion trajectories (multiple initial conditions) on the same Poincaré section. This analysis led to the identification of critical points on the phase diagram. A vigorous ion acceleration now can be explained in terms of the location of these points in the region of regular motion. A second-order perturbation analysis of the equation of motion allowed us to derive the criterion defining the allowed and forbidden acceleration domains in terms of the location of these points.

According to this analysis, for a pair of beating ($\nu_1-\nu_2=1$) electrostatic waves interacting nonlinearly with a magnetized ion, significant ion acceleration can occur as long as the Hamiltonian of the system *does not* satisfy the following ''trapping'' criterion

$$H[(\nu-\sqrt{\varepsilon})/2;\pi]<H(\rho_0;\theta_0) \\ <H(\nu-\sqrt{\varepsilon};\pi) \quad \text{with} \quad \rho_0<\nu-\sqrt{\varepsilon} \tag{23}$$

(which strictly applies when $\nu\gg 1$). If the ion's initial conditions do not satisfy the above trapping criteria, the ion can be accelerated from arbitrarily low initial velocity through the region of regular motion to the stochastic region where substantial energization can occur.

Regular ion acceleration is a much slower process than stochastic energization [4]. However, as the wave amplitude is increased, the region of stochastic motion can extend down to low initial velocities. It is important to note that the trapping criterion is in terms of the (initial) *Hamiltonian* and not just the (initial) *velocity* (ρ_0). The necessary (wave-beating) condition stated in Eq. (1) along with the avoidance of the trapping criterion stated in Eq. (23) represent two *necessary and sufficient* conditions for the beating-wave ion acceleration mechanism to occur.

While the above study offers insight into the fundamental problem of a single ion interacting with two beating waves, the relevance of the mechanism to practical problems involving a plasma rests on resolving a number of issues: (1) the effects of oblique wave propagation, as recently studied in Ref. [19]; (2) the effects of wave dispersion; and (3) the extension to collection of particles and the role of collisions. This last effect was a subject of numerical investigation in Ref. [17]. In that work we found that collisional scattering can enhance ion energization by providing an escape mechanism for the ions trapped in the forbidden acceleration domain of phase space.

ACKNOWLEDGMENT

The authors acknowledge the valuable insight that resulted from their conversations with Professor Philip Holmes.

APPENDIX: $S_6^{\nu_i,\nu_j}(\rho)$ TERM SIMPLIFICATION

Using Eq. (1) and substituting for $J_m(\rho)$ and $J'_m(\rho)$ with the identities [18]

$$J_{m-1}(\rho)+J_{m+1}(\rho)=\frac{2m}{\rho}J_m(\rho), \\ J_{m-1}(\rho)-J_{m+1}(\rho)=J'_m(\rho), \tag{A1}$$

we can rewrite $S_6^{\nu_i,\nu_j}(\rho)$ as

$$S_6^{\nu_i,\nu_j}(\rho)=\frac{1}{8}\left\{\sum\frac{J_{m+2}(\rho)J_{m+1}(\rho)}{\nu-m}+\sum\frac{J_m(\rho)J_{m+1}(\rho)}{\nu-m} \right. \\ -\sum\frac{J_{m-1}(\rho)J_{m+2}(\rho)}{\nu-m}-\sum\frac{J_m(\rho)J_{m-1}(\rho)}{\nu-m} \\ +\sum\frac{J_{m-1}(\rho)J_{m-2}(\rho)}{\nu-m}+\sum\frac{J_{m+1}(\rho)J_{m-2}(\rho)}{\nu-m} \\ \left.-\sum\frac{J_m(\rho)J_{m-1}(\rho)}{\nu-m}-\sum\frac{J_m(\rho)J_{m+1}(\rho)}{\nu-m}\right\}. \tag{A2}$$

Now we use the identity [20]

$$\sum_{m=-\infty}^{\infty}\frac{J_{m+p}(\rho)J_m(\rho)}{\nu-m}=\frac{\pi}{\sin\pi\nu}J_{p+\nu}(\rho)J_{-\nu}(\rho),$$

which is valid for $p>0$ to simplify Eq. (A2) to

$$S_6^{\nu_i,\nu_j}(\rho)=\frac{\pi}{8\sin\pi\nu}[2J_{\nu+2}(\rho)J_{-(\nu+1)}(\rho) \\ -2J_\nu(\rho)J_{-(\nu-1)}(\rho)],$$

which, with the help of identities (A1), may be easily shown to equal to

$$S_6^{\nu_i,\nu_j}(\rho)=\frac{\rho}{\nu}\frac{\pi}{\sin\pi\nu}[J_{\nu+1}(\rho)J_{-(\nu+1)}(\rho) \\ -J_{\nu-1}(\rho)J_{-(\nu-1)}(\rho)] \\ +\frac{\rho}{(\nu+1)}\frac{\pi}{\sin\pi(\nu+1)}[J_\nu(\rho)J_{-\nu}(\rho) \\ -J_{\nu+2}(\rho)J_{-(\nu+2)}(\rho)].$$

Chia *et al*. [13] showed that $S_1^{\nu_i}(\rho)$ can be simplified as

$$S_1^{\nu_i}(\rho) = \frac{\pi}{8 \sin \pi \nu_i} [J_{\nu_i+1}(\rho) J_{-(\nu_i+1)}(\rho) - J_{\nu_i-1}(\rho) J_{-(\nu_i-1)}(\rho)].$$

It is then clear that

$$S_6^{\nu_i,\nu_j}(\rho) = \frac{\rho}{\nu_i} S_1^{\nu_i}(\rho) + \frac{\rho}{\nu_j} S_1^{\nu_j}(\rho). \quad \text{(A3)}$$

Finally, we caution that relation (A3) holds only for the special case of $\nu_i \neq$ integer and $\nu_j = \nu_i + 1$.

[1] A. Ram, A. Bers, and D. Benisti, J. Geophys. Res. **103**, 9431 (1998).
[2] D. Benisti, A. Ram, and A. Bers, Phys. Plasmas **5**, 3224 (1998).
[3] D. Benisti, A. Ram, and A. Bers, Phys. Plasmas **5**, 3233 (1998).
[4] E. Choueiri and R. Spektor, *Coherent Ion Acceleration Using Two Electrostatic Waves* (AIAA, Washington, D.C., 2000), AIAA-2000-3759.
[5] A. Lichtenberg and M. Lieberman, *Regular and Stochastic Motion*, Applied Mathematical Sciences, Vol. 38 (Springer-Verlag, New York, 1983).
[6] R. Grimshaw, *Nonlinear Ordinary Differential Equations* (Blackwell, Oxford, 1990).
[7] C. Karney, Phys. Fluids **21**, 1584 (1978).
[8] G. Smith and A. Kaufman, Phys. Rev. Lett. **34**, 1613 (1975).
[9] A. Fukuyama, H. Momota, R. Itatani, and T. Takizuka, Phys. Rev. Lett. **38**, 701 (1977).
[10] C. Karney and A. Bers, Phys. Rev. Lett. **39**, 550 (1977).
[11] G. Zaslavsky, R. Sagdeev, D. Usikov, and A. Chernikov, *Weak Chaos and Quasi-Regular Patterns* (Cambridge University Press, Cambridge, 1991).
[12] F. Skiff, F. Anderegg, and M. Tran, Phys. Rev. Lett. **58**, 1430 (1987).
[13] P.-K. Chia, L. Schmitz, and R. Conn, Phys. Plasmas **3**, 1545 (1996).
[14] H. Goldstein, *Classical Mechanics* (Addison-Wesley, Cambridge, MA, 1951).
[15] A. Deprit, Celest. Mech. **1**, 12 (1969).
[16] R. Candy and W. Rozmus, Physica D **52**, 267 (1991).
[17] R. Spektor and E. Choueiri, *Effects of Ion Collisions on Ion Acceleration by Beating Electrostatic Waves* (The Electric Rocket Propulsion Society, Worthington, OH, 2001), IEPC-03-65.
[18] G. Watson, *A Treatise on the Theory of Bessel Functions*, 2nd ed. (Cambridge University Press, Cambridge, 1962).
[19] D. Strozzi, A. Ram, and A. Bers, Phys. Plasmas **10**, 2722 (2003).
[20] G. Zaslavskii, R. Sagdeev, D. Usikov, and A.A. Chernikov, Usp. Fiz. Nauk **156**, 887 (1988) [Sov. Phys. Usp. **31**, 887 (1988)].